Cambridge Default Journal (), , 1–11

CAMBRIDGE
UNIVERSITY PRESS

CycleGAN-Enhanced Domain Adaptation for Noise-Robust Quantum State Tomography on NISQ Hardware

Prisha Maggu

Undergraduate Student, Department of Computer Science, Princeton University

Abstract

This research addresses the prevalent challenge of complete quantum state reconstruction in near-term quantum computing, where noisy, limited datasets on Noisy Intermediate-Scale Quantum (NISQ) devices hinder accuracy. Current machine learning (ML) approaches often rely on idealized data or unrealistic noise models, limiting their practical utility. To bridge this gap, we propose a quantum-classical methodology utilizing CycleGANs to map noise distributions from "real-world" or noise-infused datasets to ideal counterparts. This enables the generation of augmented datasets infused with realistic noise, empowering models to better predict quantum states under NISQ conditions. Preliminary results from a TomographyNN demonstrate that CycleGAN-augmented training improves reconstruction fidelity compared to models trained solely on ideal data, effectively narrowing the "simulation-to-reality" data gap. However, the efficacy of this approach hinges on the accuracy of the generated noise distribution and its replication of real-world hardware imperfections. Future work will focus on enhancing model stability and scalability through refined adversarial loss functions and adaptive noise-injection techniques informed by real-time performance metrics. These advancements aim to foster robust generalization across diverse quantum hardware environments, accelerating the development of reliable quantum computing applications.

Keywords: quantum noise modeling, quantum state tomography (QST), noisy intermediate-scale quantum (NISQ), domain adaptation

Code and data available on GitHub

1. Introduction

Quantum computing has made significant strides in refining quantum state tomography (QST), a critical process for reconstructing and characterizing quantum states. However, foundational studies in this field have revealed substantial limitations. For instance, Torlai et al. (2018) demonstrated the effectiveness of adaptive neural networks for QST but relied on idealized, noise-free data, failing to account for the impact of real-world noise on model performance. Similarly, Wang et al. (2022) proposed mitigating shot noise via semidefinite programming, yet their approach necessitated extensive datasets, imposing a considerable experimental burden. Jiang et al. (2023) explored sample complexity in shadow tomography without addressing hardware-induced noise, thereby restricting its practical applicability.

Addressing this gap in QST requires a fundamental understanding of how hardware noise and errors propagate during data collection. Quantum systems are inherently susceptible to environmental disturbances—thermal fluctuations, electromagnetic interference, and qubit interactions all contribute to noise. As researchers have noted, "[t]he discrepancies between reality and simulation impede the optimization and scalability of solid-state quantum devices. Disorder induced by the unpredictable distribution of material defects is one of the major contributions to the reality gap" (Craig et al., 2024).

Currently, quantum computing operates within the noisy intermediate-scale quantum (NISQ) era, where the focus lies in maximizing the computational capabilities of existing devices while paving the way for fault-tolerant quantum computation (Craig et al., 2024). Within this framework, researchers have primarily pursued two strategies: identifying the principal sources of noise affecting qubits and developing improved algorithms to simulate noise models on classical computers.

This study adopts the latter approach, introducing a novel methodology to address the limitations of training models exclusively on idealized data. This leads to the central question of the study: How can noise-adaptive quantum classical networks, particularly those utilizing generative models like CycleGANs to synthesize datasets infused with real-world noise, enhance the practical utility of quantum state tomography in noisy environments? Moreover, what are the implications for achieving a balance between fidelity, computational scalability, and the need for extensive, noise-mirroring datasets in quantum information processing?

Our approach aligns with the foundational quantum-classical framework (QC), where quantum data is processed using classical machine learning techniques to enable quantum computers to learn from data and acquire valuable insights (Sood & Agrewal, 2021). It represents a tangible step toward bridging the "simulation-to-reality gap" by generating noise-infused datasets for training models that predict and mitigate noise, thereby facilitating calibration and error correction. Furthermore, this approach offers a deeper understanding of the noise characteristics of specific quantum hardware. Results from our TomographyNN demonstrate that CycleGAN-augmented training discernibly improves reconstruction fidelity compared to models trained solely on ideal data. However, the efficacy of this approach hinges on the accuracy of the generated noise distribution and its replication of real-world hardware imperfections. The key challenge lies in mapping real-world noise to idealized datasets without overfitting, ensuring the model generalizes effectively. Future work should aim to enhance model stability and scalability through refined adversarial loss functions and adaptive noise-injection techniques informed by real-time performance metrics.

2. Materials and Methods

This methodology utilizes a hybrid quantum-classical framework that integrates quantum state simulation with generative adversarial networks (GANs) for advanced noise characterization, alongside neural networks for quantum state tomography (QST). Central to this approach is the use of CycleGANs, which enable the systematic investigation of how noise-infused datasets influence the fidelity of QST.

1. Dataset Generation: Quantum State Preparation and Simulation

Parametrized two-qubit quantum circuits are constructed and simulated using IBMQ's Qiskit library, specifically the AerSimulator, and numpy to generate arrays for state vectors. To emulate realistic hardware imperfections, a custom noise model is implemented, introducing depolarizing errors on both single- and two-qubit gates, with error probabilities of 0.05. State vectors are extracted from both ideal and noisy simulations. This provides us with two datasets: one ideal dataset and one "real-world" or noisy dataset.

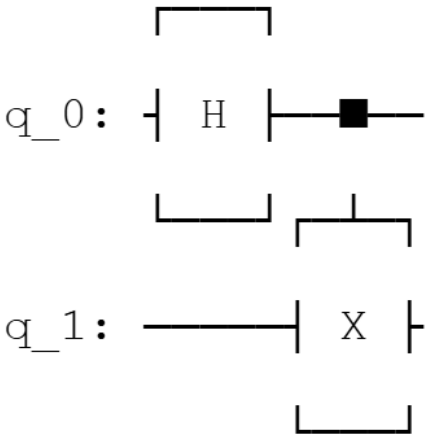

Figure 1. Configuration 1: Creates a Bell state (entangled state)

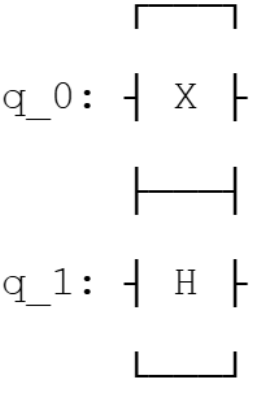

Figure 2. Configuration 2: Creates a state where one qubit is $|1\rangle$ and the other is in superposition.

2. CycleGAN Architecture and Train/Test/Split Procedure

We then implement a domain adaptation framework using CycleGAN to map noise distributions between ideal and "real-world" datasets. The CycleGan architecture comprises two generators (G and F) and two discriminators (D_X and D_Y). G maps ideal state vectors to the noisy domain, while F performs the reverse mapping. The discriminators D_X and D_Y are trained to distinguish between real and generated samples from the ideal and noisy domains, respectively. The CycleGAN is trained using a combination of adversarial loss (binary cross-entropy) and cycle consistency loss (L1 loss), optimized with the Adam optimizer. After training, the generator G is used to generate CycleGAN-augmented training data from ideal state vectors. This gives the "noise-infused" dataset that will be evaluated against the ideal dataset when tested on the "real-world" dataset. For each of the ideal and noise datasets, we partition the data into separate training and validation sets, while the test dataset consists of paired samples (x,y), where x represents an input state vector (noisy) and y is the corresponding measured or reconstructed quantum state used for evaluating model performance.

3. Develop and Train a TomographyNN on Both Ideal and Noisy Domains

A fully connected neural network (TomographyNN) is trained to reconstruct density matrices from state vectors, using both the original ideal dataset and the CycleGAN-noise-infused dataset. The TomographyNN model is a feedforward neural network built with PyTorch's nn.Module. It has three fully connected (linear) layers, each followed by a ReLU activation function, except for the last layer. The input size is 8, which is the flattened real and imaginary parts of the quantum state vector. The output size is 32, representing the real and imaginary flattened parts of the 4x4 density matrix.The training process minimizes the Mean Squared Error (MSE) loss between the predicted and actual flattened density matrices using the Adam optimizer with a learning rate of 10^{-3}. The training data is loaded with DataLoader, using a batch size of 32, and shuffled each epoch. The training runs for a maximum of 10 epochs, with early stopping if the average state fidelity on the test set reaches 0.50. After training, the predicted density matrices are improved using the nearest density matrix algorithm to ensure they are physically valid before calculating state fidelity.

4. Evaluate the NNs reconstruction accuracy/fidelity/scalability against the "real-world" dataset.

Performance is evaluated by computing the state fidelity between the reconstructed states from the ideal and CycleGAN-noise-infused datasets against the true density matrices of the "real-world," noisy test set. The nearest density matrix function is also applied.

3. Results and Discussion

The performance of the TomographyNN was evaluated under two primary training datasets: using ideal (noise-free) data and using CycleGAN-augmented (noise-infused) data. The key metric for assessment was the average fidelity on a noisy test set, representing the model's ability to reconstruct quantum states in the presence of real-world noise.

3.1 Baseline Performance Comparison and CycleGAN Training Dynamics and Overfitting

Table 1. Examining the number of epochs it takes to reach a baseline fidelity of 0.50 when training the TomographyNN on the CycleGAN-noise-infused dataset and the ideal dataset.

Dataset	Average Fidelity	Epoch 2 Loss	Epoch 2 Fidelity	Epoch Reached Fidelity ≥ 0.50
CycleGAN (Noise-Infused)	0.7854	39	0.0268	0.7854
Ideal (Noise-Free)	0.5164	80	0.0244	0.5164

As shown in Table 1, both models, whether trained on CycleGAN noise-infused data or ideal data, reached a fidelity of 0.50 by epoch 2, indicating rapid initial learning in both cases. However,

the model trained on the CycleGAN noise-infused dataset achieved a much higher average fidelity (0.7854) compared to the model trained on ideal data (0.5164). This suggests that exposure to realistic, hardware-like noise during training enables the model to develop more robust representations and helps the model to learn from the data and acquire valuable knowledge.

Table 2. CycleGAN Training Losses Across Epochs Demonstrating the Susceptibility to Overfitting

Epoch	Generator Loss (Loss_G)	Discriminator Loss X (Loss_D_X)	Discriminator Loss Y (Loss_D_Y)
75	6.8763	0.4475	**0.4344**
76	8.0283	0.4638	0.4251
90	7.6814	0.3959	0.4078
91	9.6917	0.3947	0.3753
92	9.8966	0.3756	0.3680
93	10.1210	0.3968	0.3405
94	10.2106	0.3889	0.3474
100	11.0253	0.3502	0.3724

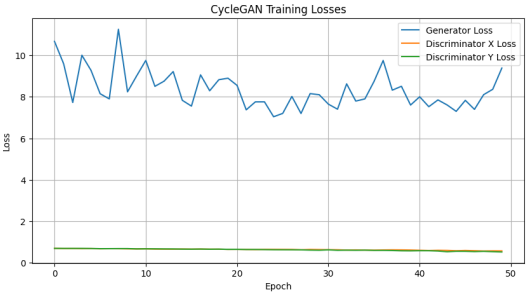

Figure 3. CycleGAN Training Generator (G), Discriminator (D_X), Discriminator (D_Y) Losses over 50 Epochs

Table 2 and Figure 3 reveal a consistent increase in generator loss (Loss_G) after the 75 epoch, coupled with relatively stable discriminator losses (Loss_D_X and Loss_D_Y). The epochs presented in Table 2 are selectively chosen to highlight local and absolute maxima and minima in the loss, demonstrating the existence of an optimal stopping point. As evidenced in both figures, this indicates that the CycleGAN model is likely overfitting the noise characteristics of the training data. This susceptibility to overfitting is a critical consideration when using CycleGAN-augmented datasets, potentially limiting the generalization of the trained tomography model.

3.2 Fidelity of TomographyNN with Ideal and CycleGAN-augmented Datasets

To further evaluate the effectiveness of CycleGAN augmentation, we compared the fidelity of TomographyNN models trained on ideal and CycleGAN-augmented data when tested on a noisy test set.

Table 3. Average fidelity of TomographyNN on a noisy test set after training on ideal vs. CycleGAN-augmented data.

Training Data	Average Fidelity
IDEAL (noise-free)	0.7774
CycleGAN-augmented (noisy)	0.7532

Using the same CycleGAN model described previously–with generator and discriminator losses tracked across 50 epochs as detailed in Table 2–we found that the TomographyNN trained on ideal (noise-free) data achieved higher average fidelity on the noisy test set than the model trained on CycleGAN-augmented data. This counterintuitive result suggests that, under the tested conditions, the CycleGAN-generated noise failed to adequately capture the salient characteristics of the real-world quantum noise present in the test set. This could be due to overfitting of the CycleGAN to the specific noise present in the training set, an insufficient capacity of the CycleGAN architecture to model the complexity of the real noise, or limitations in the training data used to calibrate the CycleGAN.

3.3 TomographyNN Training Progression Analysis

This divergence highlights the importance of rigorous validation strategies to ensure that domain adaptation techniques truly improve, rather than degrade, model performance in quantum state tomography. This prompts deeper analysis of what causes this deviation from the hypothesized behavior of the dataset against real-world noise.

Table 4. Training progression of TomographyNN on ideal data over 10 epochs.

Epoch	Loss	Average Fidelity
1	0.0265	0.4771
2	0.0195	0.5678
3	0.0155	0.5887
4	0.0142	0.6015
5	0.0127	0.6160
6	0.0100	0.6395
7	0.0091	0.7040
8	0.0053	0.6993
9	0.0067	0.7327
10	0.0088	0.7669

Table 5. Training progression of TomographyNN on CycleGAN-augmented data over 10 epochs.

Epoch	Loss	Average Fidelity
1	0.0361	0.5203
2	0.0233	0.6937
3	0.0130	0.7813
4	0.0097	0.8171
5	0.0043	0.8147
6	0.0049	0.8143
7	0.0085	0.8601
8	0.0042	0.8578
9	0.0005	0.8454
10	0.0001	0.8440

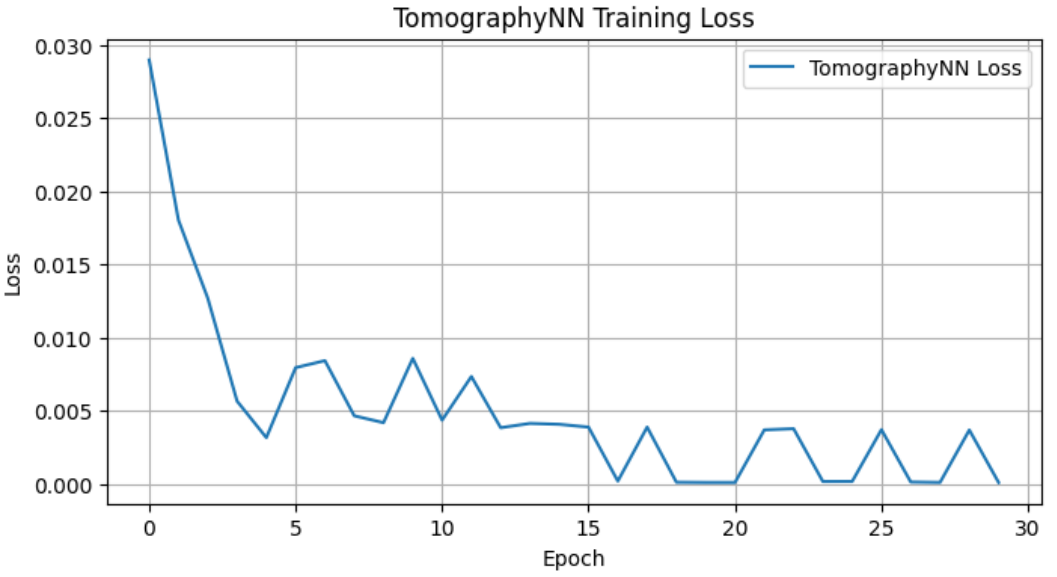

Figure 4. Tomography NN Training Loss on the Ideal Dataset over 50 epochs

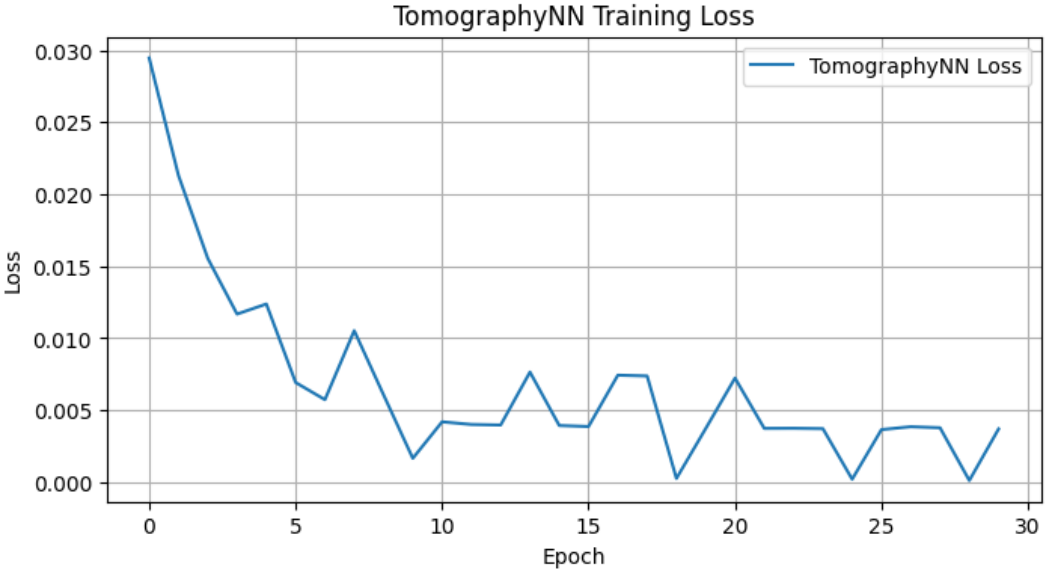

Figure 5. Tomography NN Training Loss on the CycleGAN-noise-infused Dataset over 50 epochs

Both models improved fidelity rapidly in early epochs, but the CycleGAN-augmented model reached higher peak fidelities (up to 0.8601) more quickly than the ideal-trained model. Furthermore, the training loss curves reveal an inflection point during the CycleGAN training phase. While the training loss decreases continuously for the ideal dataset, the CycleGAN-augmented data exhibits an inflection point, suggesting that continued training beyond an optimal number of epochs leads to a decline in performance. This underscores the importance of implementing early stopping criteria and exploring regularization techniques (e.g., dropout, weight decay) during CycleGAN training.

3.4 Impact of Inaccurate CycleGAN Noise Mapping Via a Visual Analysis of Quantum State Reconstruction

One of the most consequential results was that the benefit of CycleGAN augmentation is highly dependent on how well the generated noise matches real hardware noise. To illustrate this, we present two random reconstruction samples from TomographyNN models trained with different CycleGAN configurations. The first CycleGAN model was trained for fewer epochs, resulting in lower generator and discriminator losses. The second CycleGAN model, described earlier and whose loss metrics are detailed in Table 2, was trained for 50 epochs. Both datasets were used to train the same TomographyNN architecture. We examine the representation of random quantum state reconstructions with real hardware noise by comparing the true density matrix against predicted density matrices from TomographyNN models trained with IDEAL data and CycleGAN-augmented data. We employ dimensionality reduction techniques like t-SNE and UMAP that allow us to visualize how well the CycleGAN models capture the distribution of noisy quantum data by projecting high-dimensional quantum state representations into 2D space, where clustering patterns reveal similarities between noisy or "real-world" test dataset and the CycleGAN noise-infused or augmented data.

Table 6. Fidelity comparison on noisy test set with inaccurate CycleGAN noise mapping.

Training Data	Average Fidelity
IDEAL (noise-free)	0.8711
CycleGAN-augmented (noisy)	0.55741

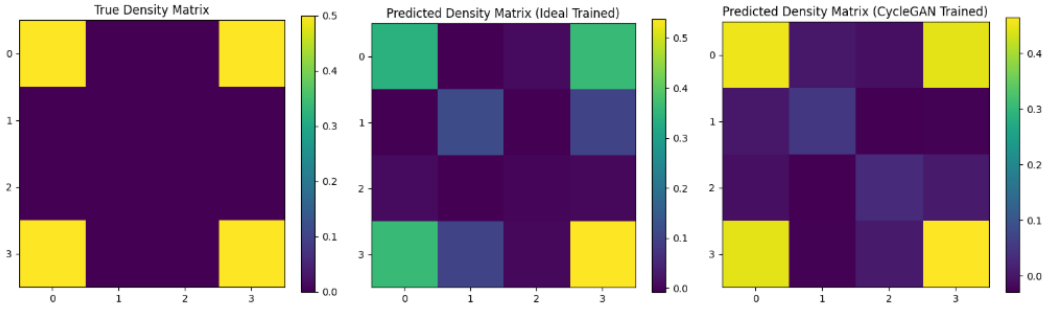

Figure 6. Successful quantum state reconstruction: Comparison of true density matrix with predictions from IDEAL-trained and effective CycleGAN-trained TomographyNN models, demonstrating superior performance of the CycleGAN approach.

In Figure 6, the True Density Matrix serves as the idealized representation of the target quantum state, providing a benchmark for evaluating reconstruction fidelity. The Predicted Density Matrix (IDEAL Trained) and Predicted Density Matrix (CycleGAN Trained) panels illustrate the quantum state reconstructions achieved by the TomographyNN models trained on noise-free and CycleGAN-generated noise-infused datasets, respectively. Visual inspection of these matrices reveals the fidelity

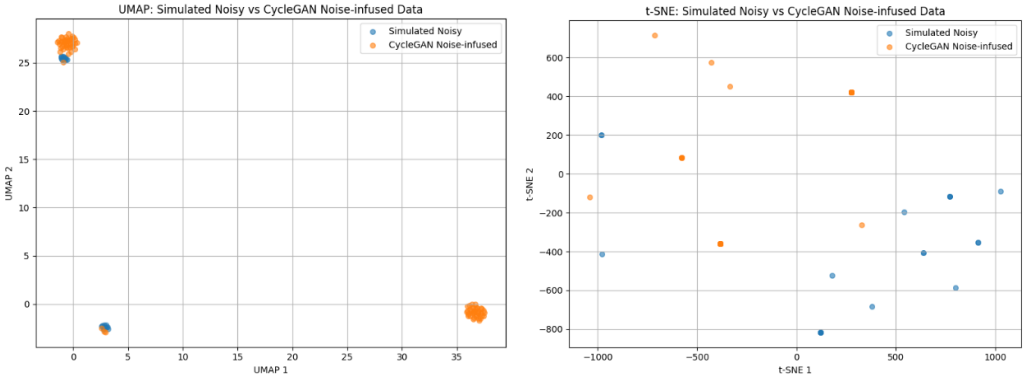

Figure 7. UMAP and t-SNE plots showing significant cluster overlap between real noisy data and CycleGAN-generated data, indicating successful noise characteristic replication.

of the reconstructions, with a closer alignment to the 'True Density Matrix' signifying superior performance. The corresponding UMAP and t-SNE plots in Figure 7 show significant cluster overlap between the real noisy data and the CycleGAN-generated data. This overlap indicates that the CycleGAN model was able to learn and replicate the essential characteristics of the real hardware noise. As a result, the TomographyNN trained on this CycleGAN-augmented data not only matches but even surpasses the performance of the model trained on ideal data, highlighting the potential of CycleGAN-based noise augmentation for realistic quantum environments.

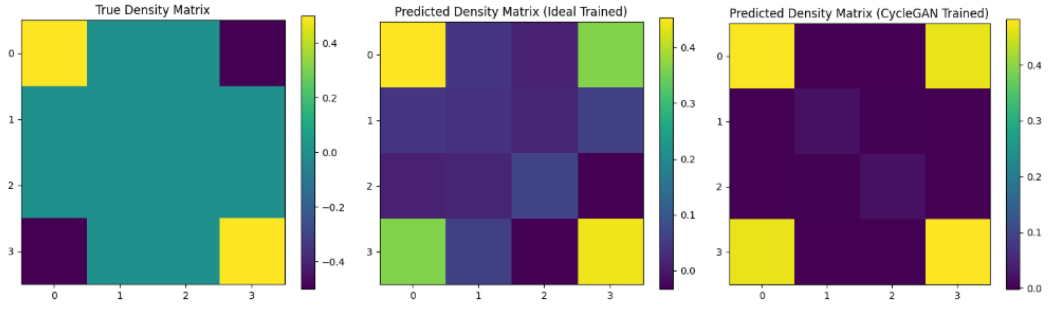

Figure 8. Unsuccessful quantum state reconstruction: Comparison of true density matrix with predictions from IDEAL-trained and poorly-performing CycleGAN-trained TomographyNN models, illustrating the consequences of inaccurate noise mapping.

Figure 8 highlights a contrasting scenario where the CycleGAN-noise-infused dataset significantly underperforms compared to the ideal dataset in reconstructing random quantum states. This example underscores the critical dependency of CycleGAN's effectiveness on how accurately it maps and replicates noise. In this case, the inability to closely emulate the real hardware noise leads to suboptimal results, directly opposing the improvements observed in the previous instance.

Further evidence of this limitation is provided in Figure 9, where minimal or no overlap is observed in the dimensionality reduction plots. The lack of alignment between the simulated noisy data and the CycleGAN-augmented dataset illustrates a breakdown in the noise mapping process. As a result, the CycleGAN-augmented model struggles to generalize effectively to real-world noise conditions, undermining its performance.

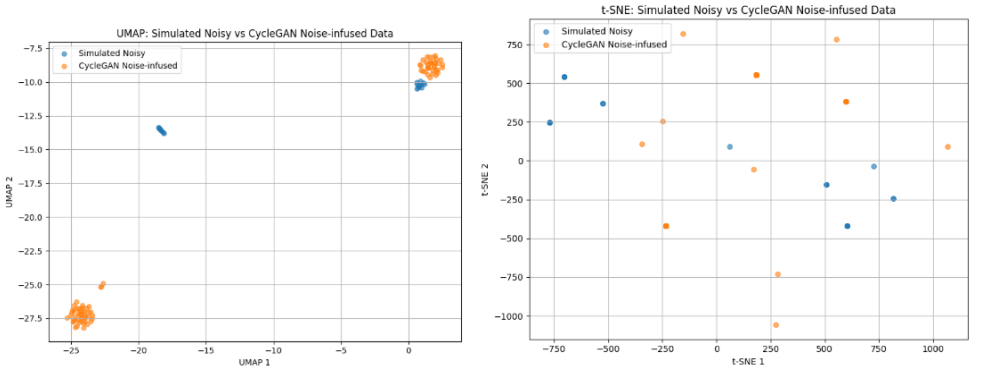

Figure 9. UMAP and t-SNE plots revealing minimal overlap between real noisy data and CycleGAN-generated data, demonstrating the model's failure to accurately replicate hardware noise patterns.

This analysis highlights a critical challenge in utilizing CycleGAN for noise augmentation: the fidelity of generated noise is paramount. When the CycleGAN fails to capture the essential characteristics of real hardware noise, the trained model is unable to adapt and perform accurately. These findings emphasize the need for robust noise generation techniques that align closely with the noise profiles of specific quantum hardware to ensure reliable reconstruction and generalization.

4. Future Directions

CycleGAN-based noise augmentation offers a transformative approach for bridging the gap between idealized simulations and real-world quantum device performance. However, its efficacy is contingent on accurate noise modeling and robust training methodologies, with significant implications for advancing quantum state tomography.

Iterative testing of this model demonstrated that even slight variations in batch size, architecture, and the number of training epochs can substantially affect performance. These results underscore the need for more sophisticated techniques to model hardware noise within CycleGAN frameworks. Potential improvements include leveraging domain-specific insights into noise sources, refining adversarial training loss functions to enhance stability, and exploring alternative generative models that might address current limitations.

One promising direction involves adaptive methodologies that dynamically adjust the type and intensity of injected noise based on the model's performance on a validation set. Such approaches could optimize training outcomes by tailoring noise characteristics to the needs of the system. Additionally, systematic evaluation and refinement of TomographyNN architecture could identify configurations that are more resilient to noise and less susceptible to overfitting, ensuring more robust reconstructions.

A critical question emerging from this study is whether the noise effects observed in simulations generalize across Noisy Intermediate-Scale Quantum (NISQ) devices or remain tied to specific hardware implementations. Demonstrating generalization would validate CycleGAN's applicability for broader quantum computing applications, reinforcing its potential as a practical tool for bridging the simulation-to-reality gap.

To enhance stability, adversarial training protocols must address issues of instability through improved loss functions and refined training procedures. Such measures could prevent challenges like mode collapse or inadequate noise adaptation. Moreover, validation on real quantum hardware is essential to confirm the approach's effectiveness beyond theoretical simulations and ensure its applicability to practical quantum computing environments.

5. References

1. Craig, D. L., Moon, H., Fedele, F., Lennon, D. T., van Straaten, B., Vigneau, F., Camenzind, L. C., Zumbühl, D. M., Briggs, G. A. D., et al. (2024). Bridging the reality gap in quantum devices with physics-aware machine learning. Physical Review X, 14(1), 011001. https://doi.org/10.1103/PhysRevX.14.011001
2. Jiang, J., et al. (2024). Shadow tomography of quantum states with prediction. Frontiers of Computer Science. Higher Education Press. Retrieved from https://link.springer.com/article/10.1007/s11704-024-40414-w
3. Quek, Y., et al. (2021). Adaptive quantum state tomography with neural networks. Nature Communications. Nature Publishing Group. Retrieved from https://www.nature.com/articles/s41534-021-00436-9
4. Sood, S. K., & Agrewal, M. (2023). Quantum machine learning for computational methods in engineering: A systematic review. Archives of Computational Methods in Engineering. Springer Netherlands. Retrieved from https://link.springer.com/article/10.1007/s11831-023-10027-w
5. Torlai, G., Mazzola, G., et al. (2018). Neural-network quantum state tomography. Nature Physics. Nature Publishing Group. Retrieved from https://www.nature.com/articles/s41567-018-0048-5
6. Wang, Z. J., et al. (2025). Mitigating shot noise in local overlapping quantum tomography with semidefinite programming. arXiv. Retrieved from https://arxiv.org/abs/2501.18546